Article

Regulation of α-synuclein by chaperones in mammalian cells

Björn M. Burmann[1,2,3,9]*, Juan A. Gerez[4,9], Irena Matečko-Burmann[1,3,5], Silvia Campioni[4,7], Pratibha Kumari[4], Dhiman Ghosh[4], Adam Mazur[1], Emelie E. Aspholm[2,3], Darius Šulskis[2,3], Magdalena Wawrzyniuk[6,8], Thomas Bock[1], Alexander Schmidt[1], Stefan G. D. Rüdiger[6], Roland Riek[4]* & Sebastian Hiller[1]*

Neurodegeneration in patients with Parkinson's disease is correlated with the occurrence of Lewy bodies—intracellular inclusions that contain aggregates of the intrinsically disordered protein α-synuclein[1]. The aggregation propensity of α-synuclein in cells is modulated by specific factors that include post-translational modifications[2,3], Abelson-kinase-mediated phosphorylation[4,5] and interactions with intracellular machineries such as molecular chaperones, although the underlying mechanisms are unclear[6–8]. Here we systematically characterize the interaction of molecular chaperones with α-synuclein in vitro as well as in cells at the atomic level. We find that six highly divergent molecular chaperones commonly recognize a canonical motif in α-synuclein, consisting of the N terminus and a segment around Tyr39, and hinder the aggregation of α-synuclein. NMR experiments[9] in cells show that the same transient interaction pattern is preserved inside living mammalian cells. Specific inhibition of the interactions between α-synuclein and the chaperone HSC70 and members of the HSP90 family, including HSP90β, results in transient membrane binding and triggers a remarkable re-localization of α-synuclein to the mitochondria and concomitant formation of aggregates. Phosphorylation of α-synuclein at Tyr39 directly impairs the interaction of α-synuclein with chaperones, thus providing a functional explanation for the role of Abelson kinase in Parkinson's disease. Our results establish a master regulatory mechanism of α-synuclein function and aggregation in mammalian cells, extending the functional repertoire of molecular chaperones and highlighting new perspectives for therapeutic interventions for Parkinson's disease.

We characterized the interactions of an array of molecular chaperones with α-synuclein on the basis of previous findings that have shown that molecular chaperones share common patterns of client recognition[10,11]. The array included human HSC70 and HSP90β, and bacterial chaperones SecB, Skp, SurA and Trigger Factor, all of which have strongly diverse architectures[10]. All of these chaperones interfered functionally with the aggregation of α-synuclein in a thioflavin T assay[6,8,12], showing effects already at a stoichiometry of 1:20 (chaperone:α-synuclein) and even stronger effects at 1:10 ratios (Fig. 1a–c). The known HSP90 inhibitors geldanamycin and radicicol (referred to hereafter as drugs) decreased the chaperoning effect of HSP90β (Fig. 1c), consistent with the known mechanism of these drugs[13,14]. We determined the segments of α-synuclein that interact with the individual chaperones at the atomic level by measuring the attenuation of the NMR signal intensity and chemical-shift perturbations using two-dimensional [^{15}N, ^{1}H]-NMR

spectroscopy. For all 6 chaperones, the effects were most pronounced for 12 amino acid residues at the N terminus and for 6 residues around Tyr39, indicating that a direct—albeit transient—intermolecular interaction occurs via these 2 segments, which are therefore identified as the canonical chaperone-interaction motif of α-synuclein (Fig. 1d–g and Extended Data Figs. 1, 2). Inhibition of HSP90β using drugs partially impaired the interaction with α-synuclein. For HSC70, the interaction was observed in the ADP-bound (HSC70$_{ADP}$) and the ATP-bound (HSC70$_{ATP}$), but not the apo, state (Fig. 1g and Extended Data Fig. 3), consistent with previous reports[6,15,16] (Supplementary Discussion). Notably, for all six chaperones, the interactions were observed at protein concentrations of 100 μM, which suggests that these interactions are unlikely to arise from nonspecific effects of macromolecular crowding. We investigated such nonspecific effects using high concentrations of either bovine serum albumin (BSA) or ubiquitin. The

[1]Biozentrum, University of Basel, Basel, Switzerland. [2]Department of Chemistry and Molecular Biology, University of Gothenburg, Gothenburg, Sweden. [3]Wallenberg Centre for Molecular and Translational Medicine, University of Gothenburg, Gothenburg, Sweden. [4]Laboratory of Physical Chemistry, Department of Chemistry and Applied Biosciences, Eidgenössische Technische Hochschule Zürich, Zurich, Switzerland. [5]Department of Psychiatry and Neurochemistry, University of Gothenburg, Gothenburg, Sweden. [6]Cellular Protein Chemistry, Bijvoet Center for Biomolecular Research and Science for Life, Utrecht University, Utrecht, The Netherlands. [7]Present address: Cellulose and Wood Materials Laboratory, Department of Functional Materials, Empa, Dübendorf, Switzerland. [8]Present address: Department of Infectious Diseases and Immunology, Utrecht University, Utrecht, The Netherlands. [9]These authors contributed equally: Björn M. Burmann, Juan A. Gerez. *e-mail: bjorn.marcus.burmann@gu.se; roland.riek@phys.chem.ethz.ch; sebastian.hiller@unibas.ch
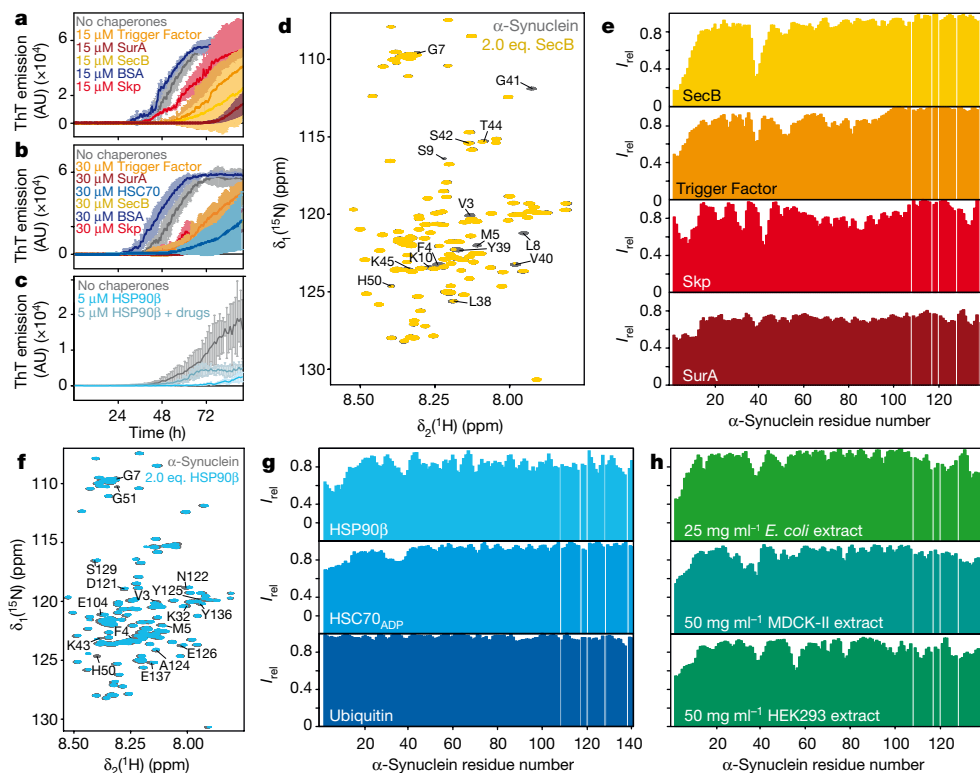
Fig. 1 | Molecular chaperones prevent aggregation through the interaction with the N terminus of α-synuclein. a, b, Thioflavin T (ThT) emission curves of 300 μM α-synuclein in the presence or absence of chaperones (15 μM (**a**) or 30 μM (**b**)). **c,** Thioflavin T emission curves of 100 μM α-synuclein in the presence of 5 μM HSP90β with and without the addition of 1 μM of drugs. **a**–**c,** Data are mean ± s.d. (*n* = 3). AU, arbitrary units. **d,** Overlay of two-dimensional [^{15}N, ^{1}H]-NMR spectra of 250 μM [*U*-^{15}N]-α-synuclein in the absence (grey) and presence (yellow) of 500 μM of SecB tetramer (*n* = 3, with similar results). **e,** Residue-resolved backbone amide NMR signal attenuation ($I_{rel} = I/I_0$) of α-synuclein upon addition of two equivalents (eq.) of SecB tetramer (yellow),

Trigger Factor dimer (orange), Skp trimer (red) or SurA dimer (dark red). **f,** Overlay of two-dimensional [^{15}N, ^{1}H]-NMR spectra of [*U*-^{15}N]-α-synuclein in the absence (grey) and presence (cyan) of two equivalents HSP90β dimer (*n* = 2, with similar results). **g, h,** Residue-resolved backbone amide NMR signal attenuation ($I_{rel} = I/I_0$) of α-synuclein upon addition of two equivalents of HSP90β dimer (cyan), HSC70$_{ADP}$ (light blue), and ubiquitin (dark blue) as well as *E. coli* cell extract (green), mammalian MDCK-II cell extract (blue) and mammalian HEK293 cell extract (green). **e, g, h,** Values that are less than 1.0 indicate intermolecular interactions.

signal was not attenuated after addition of 150–310 mg ml^{-1} ubiquitin, thus excluding the possibility that these interactions arose because of macromolecular crowding effects. For high concentrations of BSA the canonical chaperone-interaction signature is observed (Fig. 1g and Extended Data Fig. 3d–j), owing to the weak molecular chaperone function of BSA[17]. Taken together, these experiments using six chaperones and two control proteins revealed that there is a canonical chaperone interaction with α-synuclein at the N terminus and around Tyr39 that is transient in nature. Notably, it comprises the two segments of α-synuclein that are locally the most hydrophobic (Extended Data Fig. 3k, l), indicating an importance of hydrophobic residues for the interaction with chaperones.

To characterize the physiological role of chaperone–α-synuclein interactions, we determined the affinity of α-synuclein for HSC70$_{ADP}$, SecB and Skp using bio-layer interferometry. α-Synuclein binds to each of these chaperones with affinities ranging from 1 to 2 μM (Extended Data Fig. 4 and Supplementary Table 1). The ΔN-α-synuclein variant, which lacks 10 N-terminal residues, shows a decrease in affinity of two orders of magnitude, validating that this segment is part of the interaction site. At the reported cellular concentrations of α-synuclein in neuronal synapses of approximately 50 μM combined with a concentration of around 70 μM of the chaperones HSP70 and HSP90[18], about 90% of cellular α-synuclein can therefore be bound to chaperones.

We then analysed published data on the NMR intensity profiles of α-synuclein inside living mammalian cells, and found that these data feature the canonical chaperone-interaction signature[9]. Because this

pattern has been suggested to arise from interactions with cellular membranes, we first characterized α-synuclein in soluble cellular extracts, which were devoid of membranes, from *Escherichia coli* cells or mammalian HEK293 and MDCK-II cells. Notably, in each case we observed the canonical chaperone-interaction pattern (Fig. 1h and Extended Data Fig. 5a–d), indicating that this pattern does not result from the interaction with membranes. Second, we characterized the interaction pattern of α-synuclein with lipid bilayer membranes in vitro. Titrating large unilamellar vesicles (LUVs) with α-synuclein in a 125:1 lipid:protein ratio leads to a uniform decrease in the NMR signal for amino acid residues 1–90 of α-synuclein (Extended Data Fig. 6a), in agreement with previously published reports[9,19]. Adding 2–6 equivalents of SecB to solutions containing α-synuclein and LUV restored the chaperone signature, whereas the reverse experiment—that is, the addition of LUVs to an existing SecB–α-synuclein complex—led to attenuation of the NMR signal for amino acid residues 1–90 of α-synuclein, indicating that LUVs and SecB mutually compete for binding to α-synuclein (Extended Data Fig. 6). Overall, the data suggest that α-synuclein is in an equilibrium between its free state, its membrane-bound state and its chaperone-bound state, of which the last two states are mutually exclusive. The emerging hypothesis that, in mammalian cells, α-synuclein is predominantly in contact with chaperones rather than with the lipid bilayer was supported by the experimental determination of the interactome of the N terminus of α-synuclein in mammalian cells using chemical cross-linking and mass spectrometry. The interactome consists of a large number of molecular chaperones
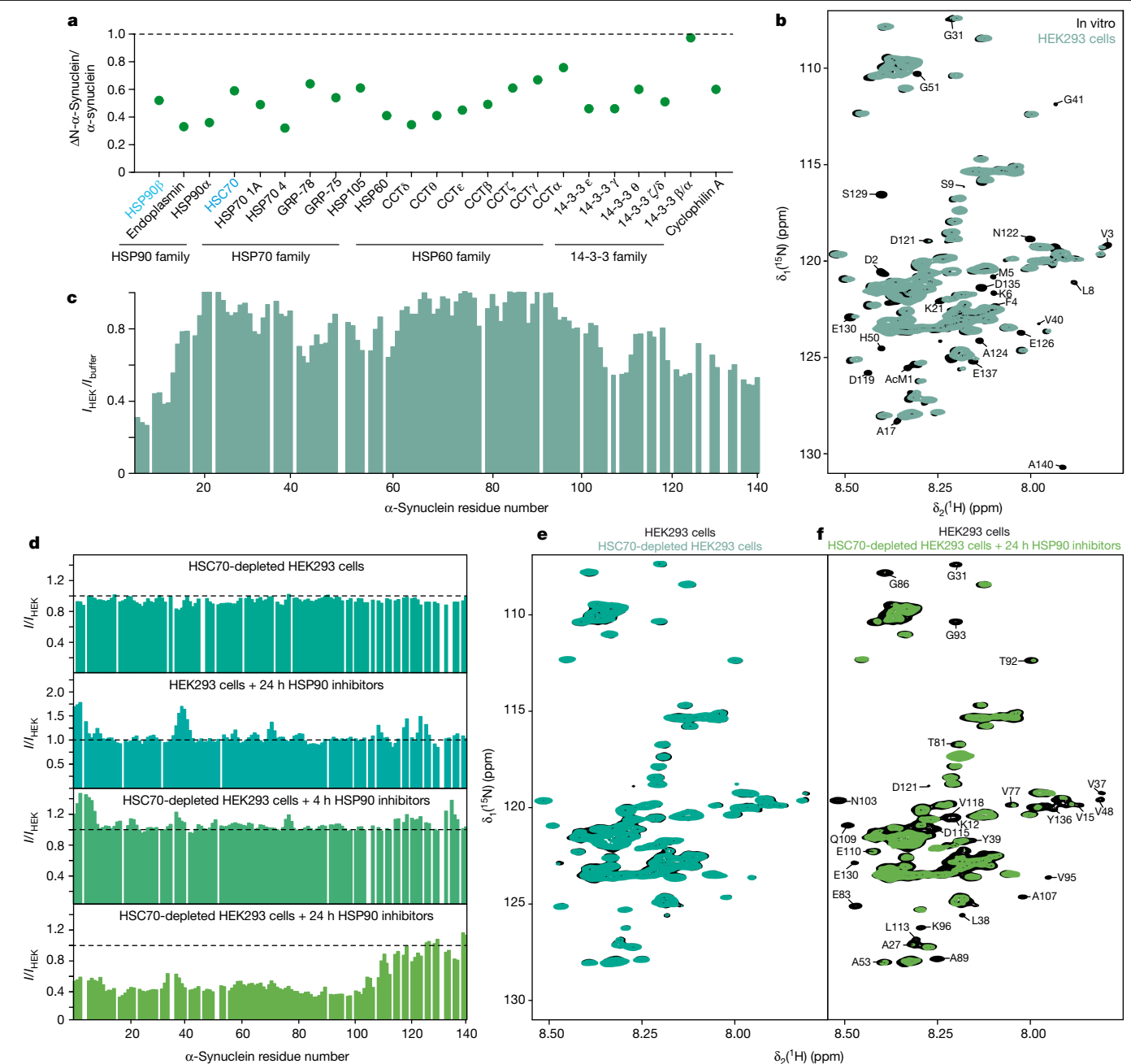
Fig. 2 | The interaction between α-synuclein and chaperones is dominant in living cells. a, Abundance ratios of proteins bound to ΔN-α-synuclein versus wild-type full-length α-synuclein determined by relative quantitative mass spectrometry (mean values, $n = 2$). **b**, Overlay of two-dimensional [^{15}N, ^{1}H]-NMR spectra of [U-^{15}N]-α-synuclein in NMR buffer (black) and inside living HEK293 cells (blue-green). Representative spectrum from $n > 5$. **c**, Residue-resolved backbone amide NMR signal attenuation (I_{HEK}/I_{buffer}) of α-synuclein in mammalian cells. **d**, NMR signal attenuation in treated cells, relative to untreated cells (I/I_{HEK}). Different combinations of HSC70 depletion and HSP90 inhibition were applied, as indicated. **e**, **f**, Overlay of two-dimensional [^{15}N, ^{1}H]-NMR spectra of [U-^{15}N]-α-synuclein in untreated HEK293 cells (black) and in HSC70-depleted HEK293 cells (green) (**e**) or in HSC70-depleted HEK293 cells after 24 h of HSP90 inhibition (green) (**f**). Representative data (**d**–**f**) for three technical replicates, with similar results.

that had abundances ranging between 30 and 75%, including several isoforms of HSP90 and six HSP70 isoforms (Fig. 2a; see Supplementary Information for details).

NMR spectroscopy in cells

Next, we carried out NMR experiments in cells to study the interaction between α-synuclein and chaperones inside living mammalian cells at atomic resolution. [U-^{15}N]-α-Synuclein was delivered into HEK293 cells at concentrations of 3–10 μM, yielding intensity patterns that are

characteristic for mammalian cell lines[9] (Fig. 2b, c), such as the canonical chaperone-interaction signature. Multiple molecular chaperones are present in the cell that have mutually overlapping functions and 'clientomes'[20]. To complement the in vitro chaperone analyses, we investigated two of the most abundant chaperones found in mammalian cells, HSC70 and HSP90β. When [U-^{15}N]-α-synuclein was delivered into HEK293 cells with reduced HSC70 levels (Extended Data Fig. 7c, d), the NMR intensity profile resembled the one observed for untreated cells, suggesting that there is functional redundancy between HSC70 and other chaperones in these cells (Fig. 2d, e). Next, we treated HEK293
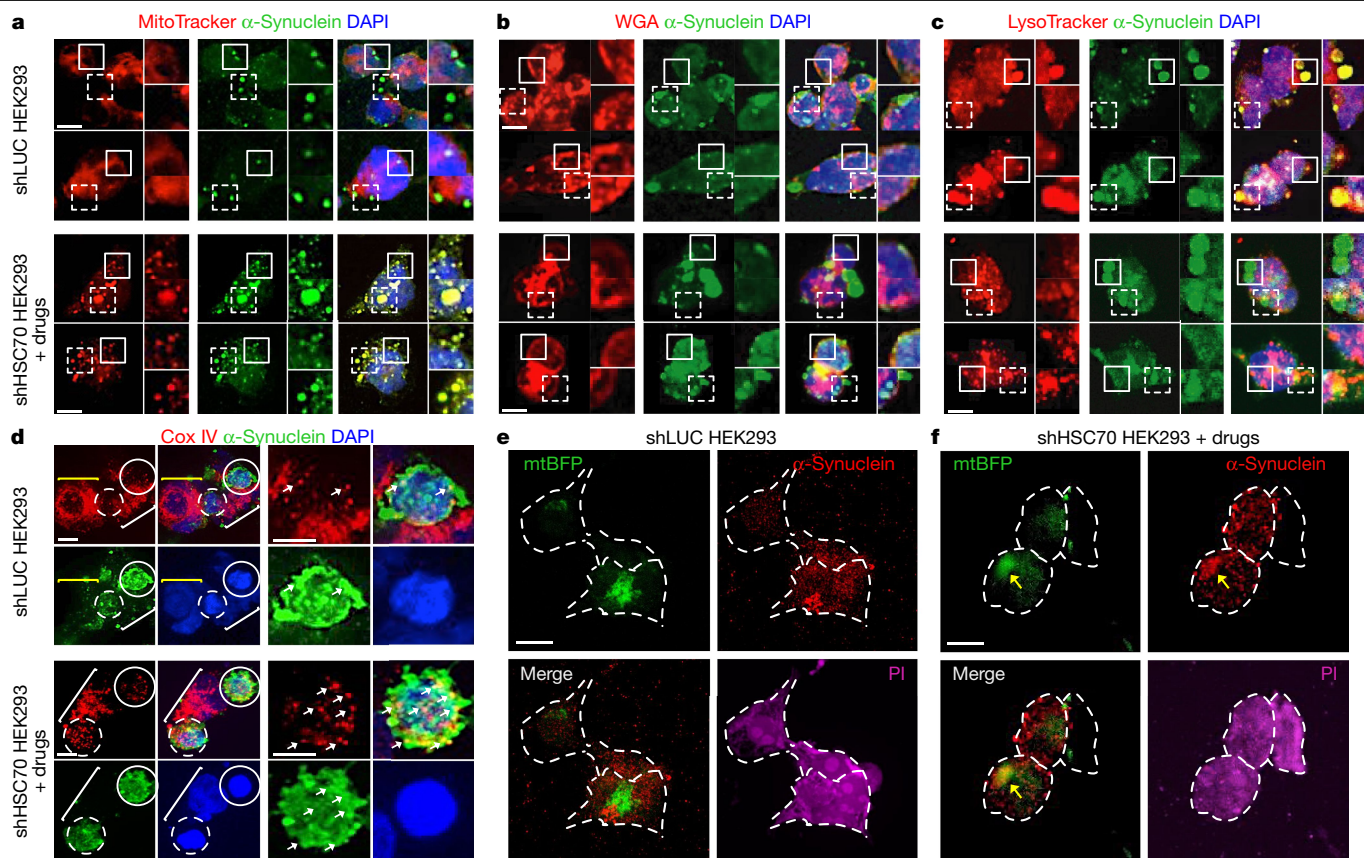
Fig. 3 | Co-localization of α-synuclein and cellular organelles assessed using immunofluorescence. a–f, Immunofluorescence analysis of α-synuclein electroporated into HEK293 cells. Cells were treated with either a control short hairpin RNA (shRNA) targeting Firefly luciferase (shLUC) or a combination of an shRNA targeting *HSC70* (shHSC70) and inhibitors of HSP90 (shHSC70 + drugs). Cells were stained with MitoTracker (red; **a**) to stain mitochondria, DAPI (blue) to stain cell nuclei, an α-synuclein-specific antibody (green) and either wheat germ agglutinin (WGA; red in **b**) to stain the plasma membrane and the endoplasmatic reticulum or LysoTracker (red in **c**) to stain acidic vesicles such as lysosomes. Outlines indicate areas of intense signal for MitoTracker and α-synuclein. Solid outlines, top magnifications; dashed outlines, bottom magnifications. **d,** Cox IV (red, mitochondrial marker) and α-synuclein (green)

were visualized by specific antibodies, nuclei were stained with DAPI (blue). Circles indicate cells with high α-synuclein content, brackets indicate cells with low α-synuclein content. Solid outlines, magnified on the right. Arrows indicate the positions of selected colocalization spots. **e, f,** Control HEK293 cells (shLUC; **e**) or HEK293 cells treated for the combined knockdown of HSC70 and inhibition of HSP90 (shHSC70 + drugs; **f**) were stably transfected with an expression plasmid containing the mitochondrial marker mtBFP. Cells were fixed and subjected to immunofluorescence analyses using an anti-α-synuclein antibody. Propidium iodide (PI) was used to stain cells to enable the visualization of cell morphology. Note, the blue colour of mtBFP was changed to green to better visualize the co-localization of mtBFP and α-synuclein. Scale bars, 10 µm. Experiments were performed twice, with similar results.

cells with the HSP90-inhibiting drugs, and found that the canonical chaperone-interaction motif showed increased intensities compared to untreated cells (Fig. 2d). This suggests that HSP90 chaperones physically and transiently interact with α-synuclein in cells, and that this interaction is lost upon drug treatment. Immunoprecipitation assays confirmed that this interaction is almost completely lost 24 h after treatment (Extended Data Fig. 7e). Finally, we simultaneously inhibited both HSC70 and HSP90, and observed a moderate effect on the canonical chaperone-interaction motif 4 h after treatment, at which point a substantial fraction of HSP90 still remains bound to α-synuclein (Extended Data Fig. 7e). At this time point, a low but measurable amount of free intracellular α-synuclein was observed (Fig. 2d). At 24 h after treatment, a marked global reduction in the signal of amino acid residues 1–90 of α-synuclein was observed, which was essentially identical to the LUV interaction pattern and to the profile that has previously been reported in which α-synuclein was bound to bacterial membranes[19,21] (Fig. 2d, f). The combined inhibition of the two types of chaperone (HSC70 and HSP90) therefore leads to a transient membrane interaction of α-synuclein, which is absent in the basal state of cells. Furthermore, in these experiments, we observed the formation of stable high-molecular-mass aggregates that contained α-synuclein (Extended Data Fig. 7f). Overall, these in-cell NMR and in vitro experiments show that, in cells,

α-synuclein transiently interacts with a pool of constitutively expressed chaperones and that this interaction predominates over the transient interaction of α-synuclein with lipid bilayer membranes. In cells such as neurons[18,22], as well as in our experiments using HEK293 cells, the concentration of chaperones is substantially larger than the concentrations of α-synuclein, highlighting the physiological relevance of these observations (Extended Data Fig. 7g, h).

Intracellular membrane localization

The interactions between α-synuclein and cellular membranes after inhibition of HSC70 and HSP90 may be a key mechanism for disease pathogenesis and we thus aimed to identify the membranous organelle that is involved using co-localization analyses. To this end, control cells and HEK293 cells depleted of HSC70 and treated with drugs for 24 h were first stained with MitoTracker (which stains mitochondria), LysoTracker (which stains acidic vesicles such as lysosomes) or Alexa-Fluor-labelled wheat germ agglutinin (which stains the plasma membrane and endoplasmic reticulum) and subsequently immunostained with anti-α-synuclein antibodies. These experiments revealed a strong colocalization of α-synuclein with mitochondria after the chaperones were depleted (Fig. 3a–c). To further confirm this association, we
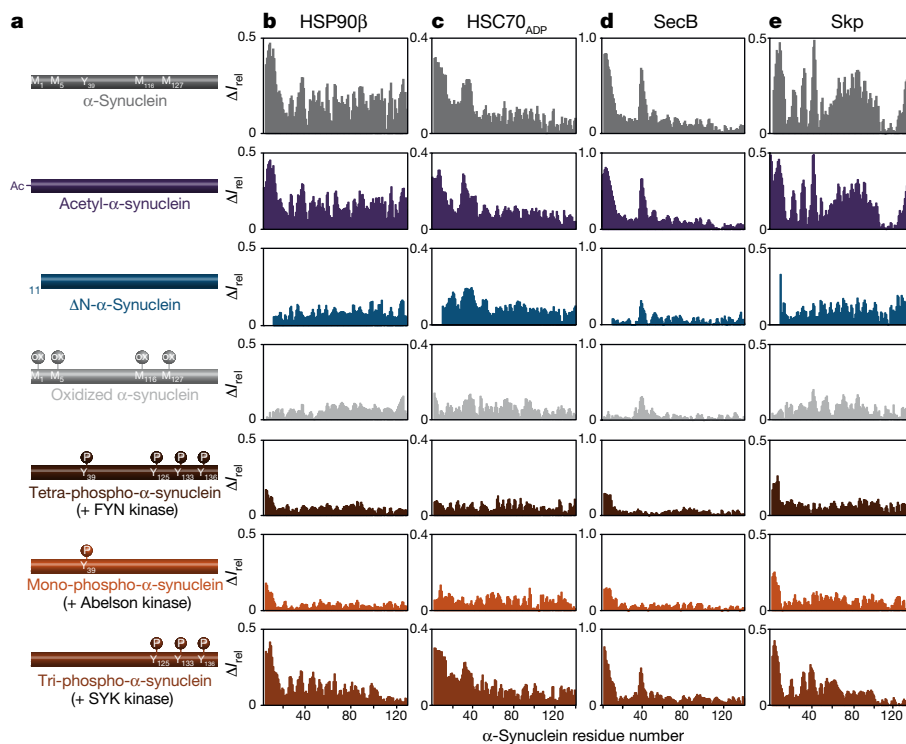
Fig. 4 | Effect of post-translational modifications on the chaperone–α-synuclein interaction. a, Modified α-synuclein variants. **b–e**, Residue-resolved backbone amide NMR signal attenuation ($\Delta I_{rel} = 1 - I/I_0$) of the α-synuclein variants upon interaction with two equivalents of HSP90β dimer (**b**), HSC70$_{ADP}$ (**c**), SecB tetramer (**d**) or Skp trimer (**e**). Increased ΔI_{rel} values are indicative of an interaction.

carried out immunofluorescence analyses using antibodies that were specific to the mitochondrial marker CoxIV and α-synuclein (Fig. 3d). In a complementary experiment, we expressed the marker mitochondrial blue-fluorescent protein (mtBFP) in control and HSC70- and HSP90-deficient HEK293 cells and stained α-synuclein with antibodies (Fig. 3e, f). Both approaches confirmed the localization of α-synuclein to mitochondria after HSC70 and HSP90 inhibition.

Effect of post-translational modifications

After establishing the canonical chaperone-interaction signature and validating its presence in living mammalian cells, we investigated the effect of chemical modifications on the α-synuclein–chaperone interaction. Using the chaperones HSP90β, HSC70$_{ADP}$, SecB and Skp, we analysed the effects of N-terminal acetylation of α-synuclein, the predominant form in mammalian cells[9,19]. N-terminal acetylation does not interfere with the interaction between α-synuclein and chaperones (Fig. 4 and Extended Data Fig. 8a–g). By contrast, ΔN-α-synuclein has a greatly reduced interaction with all chaperones, in agreement with the bio-layer interferometry experiments, and showing a synergistic effect between the N terminus and the amino acid region around Tyr39 (Fig. 4b–e). Cellular oxidative stress and an imbalance in reactive oxygen species are known hallmarks of the onset of Parkinson's disease, leading to the oxidative modification of α-synuclein[2]. Titrating of HSP90β, HSC70$_{ADP}$, SecB or Skp with methionine-oxidized α-synuclein[23] showed that oxidation of Met1 and Met5 abolish the N-terminal chaperone interaction (Fig. 4 and Extended Data Fig. 9). Next, we explored the effects of phosphorylation on the interaction with chaperones, using in vitro tyrosine phosphorylation by different kinases[5,24] (Fig. 4 and Extended Data Fig. 9). Titration of SecB, Skp, HSP90β or HSC70$_{ADP}$ with either tetra-phosphorylated or Tyr39-mono-phosphorylated α-synuclein resulted in the elimination of the chaperone interaction, whereas Tyr125-Tyr133-Tyr136-tri-phosphorylated α-synuclein showed

the chaperone-interaction pattern of unmodified α-synuclein (Fig. 4). Tyr39 phosphorylation therefore has a specific inhibitory effect on the interaction with chaperones, providing a direct rationale for in vivo studies that have shown that upregulation of Abelson kinase (c-Abl) correlates strongly with Tyr39 phosphorylation and disease progression in Parkinson's disease[5,25].

Conclusion

In summary, we have identified a functional mechanism for the regulation of α-synuclein by chaperones in mammalian cells through transient binding (Extended Data Fig. 10). Molecular chaperones bind to α-synuclein through a canonical motif, by recognizing intrinsic biophysical features at the N terminus and around Tyr39. The interaction is abrogated after inhibition of two major chaperones, and results in transient interactions of α-synuclein with cellular membranes and relocalization of α-synuclein to mitochondria. Aggregates of α-synuclein, as well as mitochondria, have been identified as major components of Lewy bodies[26,27]. We propose a model in which α-synuclein is predominantly found in a transient chaperone-interacting state in healthy cells, indicating that chaperones are a master regulator of the cellular states of α-synuclein. The model also predicts that changes in the activity or cellular levels of chaperones or α-synuclein—or the modulation of their interaction—will disturb the homeostatic balance, eventually causing or promoting Parkinson's disease. Notably, this model is in agreement with a multitude of reported experimental observations (Supplementary Discussion), including studies that have shown that the ratio of α-synuclein to chaperone is deteriorated in familial parkinsonism and that oxidative stress can lead to an increase in the phosphorylation of Tyr39 of α-synuclein[5,25], which interferes with chaperone binding. The model further shows how modulation of chaperone activity might prevent the formation of oligomeric α-synuclein, the aggregation of which leads to the disruption of the mitochondrial membrane[28], and

Article

also accounts for recent reports that impairment of mitochondria may constitute an important factor in Parkinson's disease[29–31].

Reporting summary

Further information on research design is available in the Nature Research Reporting Summary linked to this paper.

Data availability

The data that support the findings of this study are available from the corresponding authors upon request.

Online content

Any methods, additional references, Nature Research reporting summaries, source data, extended data, supplementary information, acknowledgements, peer review information; details of author contributions and competing interests; and statements of data and code availability are available at https://doi.org/10.1038/s41586-019-1808-9.

1. Goedert, M., Spillantini, M. G., Del Tredici, K. & Braak, H. 100 years of Lewy pathology. *Nat. Rev. Neurol*. **9**, 13–24 (2013).
2. Barnham, K. J., Masters, C. L. & Bush, A. I. Neurodegenerative diseases and oxidative stress. *Nat. Rev. Drug Discov*. **3**, 205–214 (2004).
3. Lashuel, H. A., Overk, C. R., Oueslati, A. & Masliah, E. The many faces of α-synuclein: from structure and toxicity to therapeutic target. *Nat. Rev. Neurosci*. **14**, 38–48 (2013).
4. Hantschel, O. & Superti-Furga, G. Regulation of the c-Abl and Bcr–Abl tyrosine kinases. *Nat. Rev. Mol. Cell Biol*. **5**, 33–44 (2004).
5. Mahul-Mellier, A. L. et al. c-Abl phosphorylates α-synuclein and regulates its degradation: implication for α-synuclein clearance and contribution to the pathogenesis of Parkinson's disease. *Hum. Mol. Genet*. **23**, 2858–2879 (2014).
6. Dedmon, M. M., Christodoulou, J., Wilson, M. R. & Dobson, C. M. Heat shock protein 70 inhibits α-synuclein fibril formation via preferential binding to prefibrillar species. *J. Biol. Chem*. **280**, 14733–14740 (2005).
7. Dimant, H., Ebrahimi-Fakhari, D. & McLean, P. J. Molecular chaperones and co-chaperones in Parkinson disease. *Neuroscientist* **18**, 589–601 (2012).
8. Pemberton, S. et al. Hsc70 protein interaction with soluble and fibrillar α-synuclein. *J. Biol. Chem*. **286**, 34690–34699 (2011).
9. Theillet, F. X. et al. Structural disorder of monomeric α-synuclein persists in mammalian cells. *Nature* **530**, 45–50 (2016).
10. Burmann, B. M., Wang, C. & Hiller, S. Conformation and dynamics of the periplasmic membrane-protein–chaperone complexes OmpX–Skp and tOmpA–Skp. *Nat. Struct. Mol. Biol*. **20**, 1265–1272 (2013).
11. He, L., Sharpe, T., Mazur, A. & Hiller, S. A molecular mechanism of chaperone–client recognition. *Sci. Adv*. **2**, e1601625 (2016).
12. Falsone, S. F., Kungl, A. J., Rek, A., Cappai, R. & Zangger, K. The molecular chaperone Hsp90 modulates intermediate steps of amyloid assembly of the Parkinson-related protein α-synuclein. *J. Biol. Chem*. **284**, 31190–31199 (2009).
13. Karagöz, G. E. et al. Hsp90–Tau complex reveals molecular basis for specificity in chaperone action. *Cell* **156**, 963–974 (2014).
14. Schopf, F. H., Biebl, M. M. & Buchner, J. The HSP90 chaperone machinery. *Nat. Rev. Mol. Cell Biol*. **18**, 345–360 (2017).
15. Roodveldt, C. et al. Chaperone proteostasis in Parkinson's disease: stabilization of the Hsp70/α-synuclein complex by Hip. *EMBO J*. **28**, 3758–3770 (2009).
16. Gao, X. et al. Human Hsp70 disaggregase reverses Parkinson's-linked α-synuclein amyloid fibrils. *Mol. Cell* **59**, 781–793 (2015).
17. Finn, T. E., Nunez, A. C., Sunde, M. & Easterbrook-Smith, S. B. Serum albumin prevents protein aggregation and amyloid formation and retains chaperone-like activity in the presence of physiological ligands. *J. Biol. Chem*. **287**, 21530–21540 (2012).
18. Wilhelm, B. G. et al. Composition of isolated synaptic boutons reveals the amounts of vesicle trafficking proteins. *Science* **344**, 1023–1028 (2014).
19. Maltsev, A. S., Ying, J. & Bax, A. Impact of N-terminal acetylation of α-synuclein on its random coil and lipid binding properties. *Biochemistry* **51**, 5004–5013 (2012).
20. Kim, Y. E., Hipp, M. S., Bracher, A., Hayer-Hartl, M. & Hartl, F. U. Molecular chaperone functions in protein folding and proteostasis. *Annu. Rev. Biochem*. **82**, 323–355 (2013).
21. McNulty, B. C., Young, G. B. & Pielak, G. J. Macromolecular crowding in the *Escherichia coli* periplasm maintains α-synuclein disorder. *J. Mol. Biol*. **355**, 893–897 (2006).
22. Cremades, N. et al. Direct observation of the interconversion of normal and toxic forms of α-synuclein. *Cell* **149**, 1048–1059 (2012).
23. Binolfi, A. et al. Intracellular repair of oxidation-damaged α-synuclein fails to target C-terminal modification sites. *Nat. Commun*. **7**, 10251 (2016).
24. Kosten, J. et al. Efficient modification of α-synuclein serine 129 by protein kinase CK1 requires phosphorylation of tyrosine 125 as a priming event. *ACS Chem. Neurosci*. **5**, 1203–1208 (2014).
25. Brahmachari, S. et al. Activation of tyrosine kinase c-Abl contributes to α-synuclein-induced neurodegeneration. *J. Clin. Invest*. **126**, 2970–2988 (2016).
26. Shahmoradian, S. H. et al. Lewy pathology in Parkinson's disease consists of crowded organelles and lipid membranes. *Nat. Neurosci*. **22**, 1099–1109 (2019).
27. Mahul-Mellier, A.-L. et al. The making of a Lewy body: the role of α-synuclein post-fibrillization modifications in regulating the formation and the maturation of pathological inclusions. Preprint at https://www.biorxiv.org/content/10.1101/500058v1 (2018).
28. Fusco, G. et al. Structural basis of membrane disruption and cellular toxicity by α-synuclein oligomers. *Science* **358**, 1440–1443 (2017).
29. Guardia-Laguarta, C., Area-Gomez, E., Schon, E. A. & Przedborski, S. Novel subcellular localization for α-synuclein: possible functional consequences. *Front. Neuroanat*. **9**, 17 (2015).
30. Park, J. S., Davis, R. L. & Sue, C. M. Mitochondrial dysfunction in Parkinson's disease: new mechanistic insights and therapeutic perspectives. *Curr. Neurol. Neurosci. Rep*. **18**, 21 (2018).
31. Reeve, A. K. et al. Mitochondrial dysfunction within the synapses of substantia nigra neurons in Parkinson's disease. *NPJ Parkinsons Dis*. **4**, 9 (2018).
32. Korndörfer, I. P., Dommel, M. K. & Skerra, A. Structure of the periplasmic chaperone Skp suggests functional similarity with cytosolic chaperones despite differing architecture. *Nat. Struct. Mol. Biol*. **11**, 1015–1020 (2004).
33. Ferbitz, L. et al. Trigger factor in complex with the ribosome forms a molecular cradle for nascent proteins. *Nature* **431**, 590–596 (2004).
34. Saio, T., Guan, X., Rossi, P., Economou, A. & Kalodimos, C. G. Structural basis for protein antiaggregation activity of the trigger factor chaperone. *Science* **344**, 1250494 (2014).
35. Bull, H. B. & Breese, K. Surface tension of amino acid solutions: a hydrophobicity scale of the amino acid residues. *Arch. Biochem. Biophys*. **161**, 665–670 (1974).
36. Rüdiger, S., Germeroth, L., Schneider-Mergener, J. & Bukau, B. Substrate specificity of the DnaK chaperone determined by screening cellulose-bound peptide libraries. *EMBO J*. **16**, 1501–1507 (1997).
37. Banerjee, P. R., Moosa, M. M. & Deniz, A. A. Two-dimensional crowding uncovers a hidden conformation of α-synuclein. *Angew. Chem. Int. Edn* **55**, 12789–12792 (2016).

Author contributions B.M.B. expressed and purified chaperones, and performed NMR experiments. B.M.B. and S.C. expressed and purified α-synuclein variants with help of P.K. E.E.A. and D.Š. supported protein purification of chaperones as well as α-synuclein variants. J.A.G. prepared and performed in-cell NMR experiments as well as chaperone knockdown experiments and immunofluorescence experiments. S.C. and D.G. performed the aggregation assays. I.M.-B. performed cell-culture experiments, prepared lipid vesicles, performed and analysed mass spectrometry experiments together with T.B. and A.S. A.M. performed model calculations. M.W. and S.G.D.R. provided purified HSP90β for interaction studies. B.M.B., S.C., R.R. and S.H. designed the study, analysed the data and wrote the manuscript with input from all co-authors.

Competing interests The authors declare no competing interests.

Additional information
Supplementary information is available for this paper at https://doi.org/10.1038/s41586-019-1808-9.
Correspondence and requests for materials should be addressed to B.M.B., R.R. or S.H.
Peer review information *Nature* thanks Gary J. Pielak and the other, anonymous, reviewer(s) for their contribution to the peer review of this work.
Reprints and permissions information is available at http://www.nature.com/reprints.
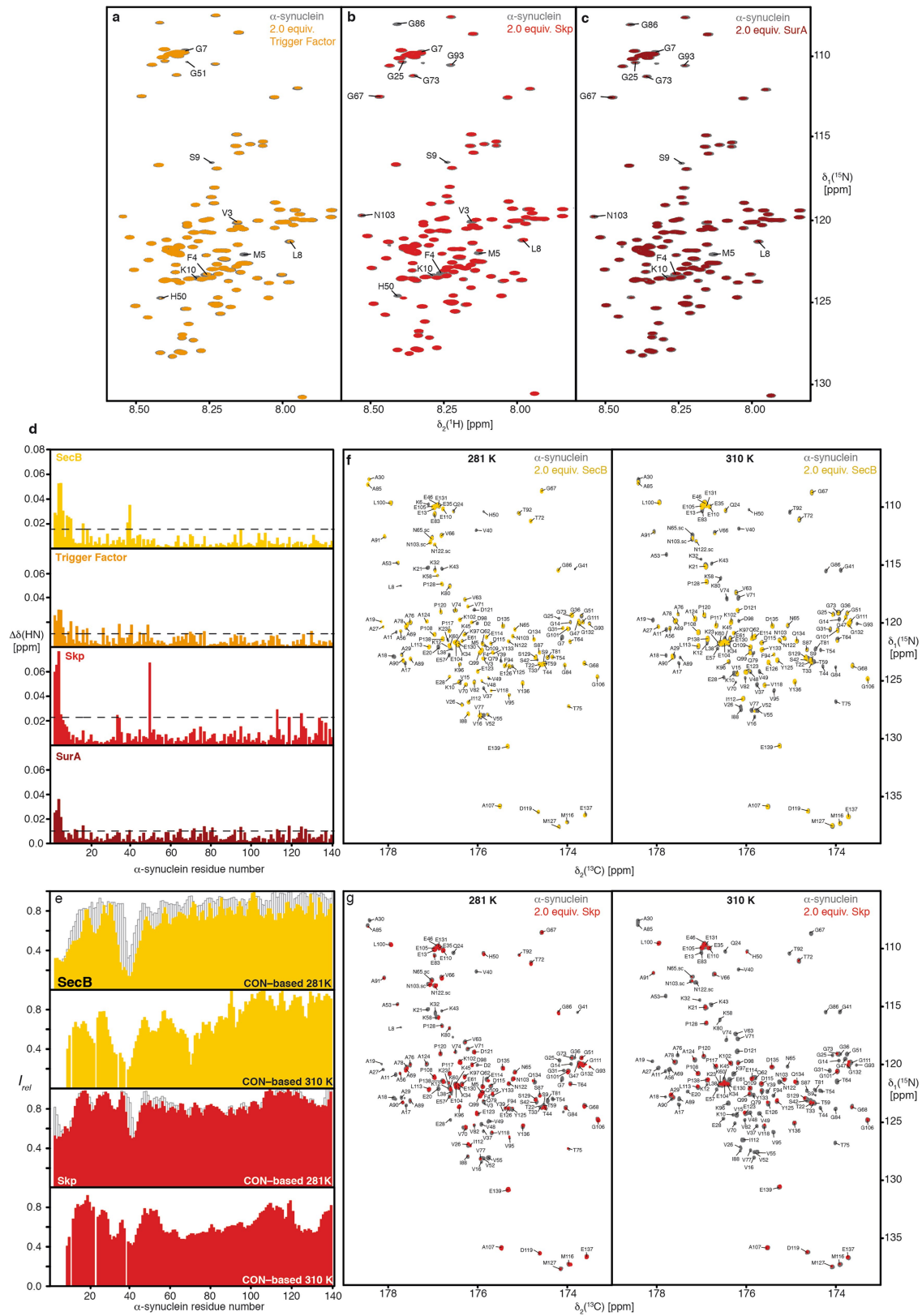
Extended Data Fig. 1 | See next page for caption.

Extended Data Fig. 1 | Interaction between α-synuclein and bacterial chaperones. a–c, Overlay of two-dimensional [^{15}N, ^{1}H]-NMR spectra of 250 μM [*U*-^{15}N]-α-synuclein in the absence (grey) and presence (orange, red or dark red) of 500 μM chaperones. The sequence-specific assignments for significantly affected resonances are indicated. **d**, Residue-resolved chemical-shift perturbations of α-synuclein caused by the addition of two equivalents of SecB tetramer (yellow), Trigger Factor dimer (orange), Skp trimer (red) or SurA dimer (dark red). Broken lines indicate a significance level of two s.d. from the mean. **e**, Temperature dependence of the α-synuclein interaction with either SecB (yellow) or Skp (red) monitored by residue-resolved intensity ratios ($I_{rel} = I/I_0$) of ^{13}C-direct-detected two-dimensional [^{15}N, ^{13}C]-NMR spectra. The intensity ratios of two-dimensional [^{15}N, ^{1}H]-NMR spectra at 281 K (Fig. 1c) are shown as an outline (grey). **f, g**, Overlay of two-dimensional [^{13}C, ^{15}N]-NMR spectra of 500 μM [*U*-^{13}C, ^{15}N]-α-synuclein in the absence (grey) and presence of 1 mM of SecB tetramer (**f**; yellow) or 1 mM of Skp trimer (**g**; red). Experiments were performed at 281 K and 310 K as indicated. The sequence-specific resonance assignment is shown. Experiments in **a–c**, **f, g** were done in duplicates, with similar results.
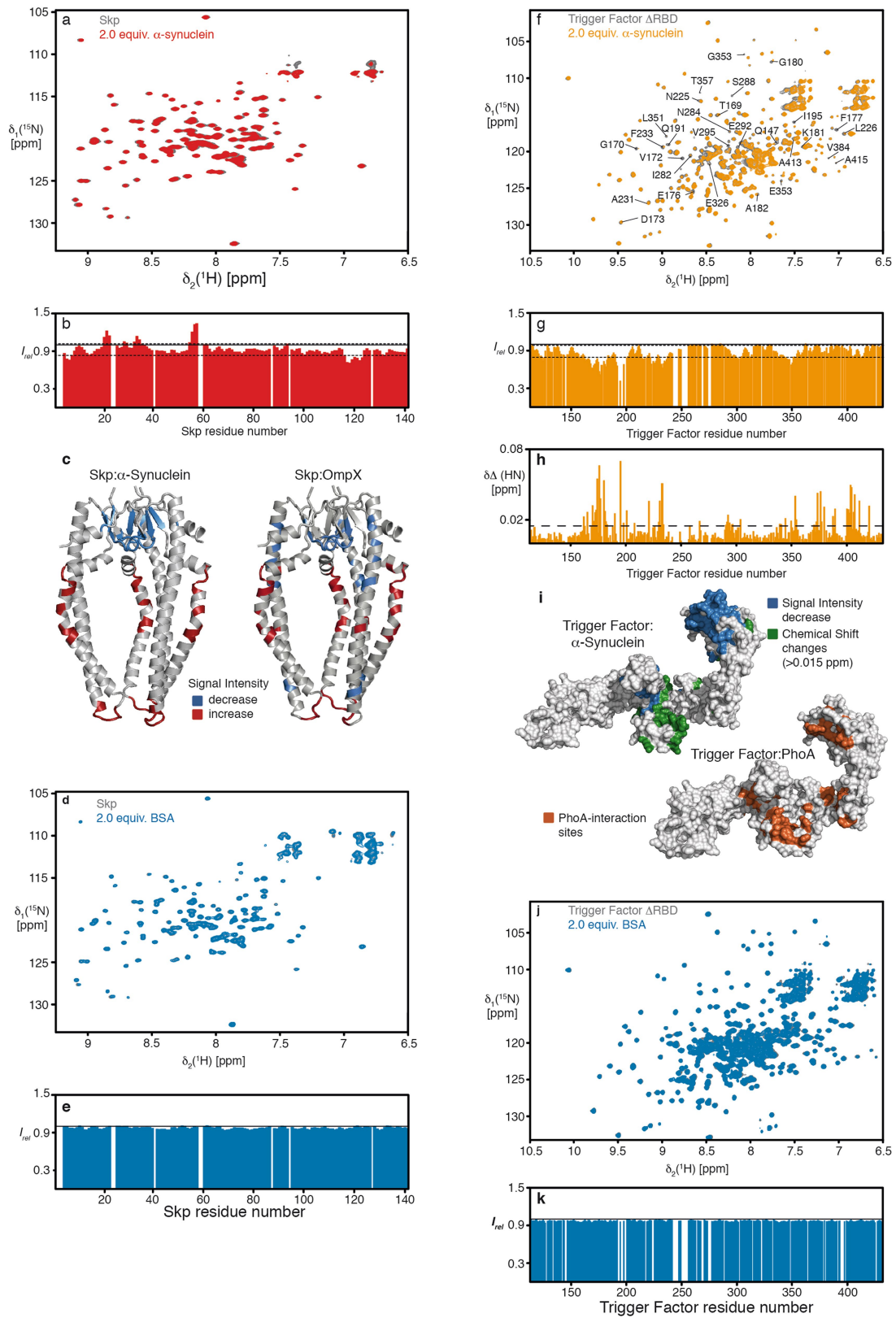
Extended Data Fig. 2 | See next page for caption.

Extended Data Fig. 2 | Chaperones Skp and Trigger Factor bind α-synuclein at their native client sites. a, Overlay of two-dimensional [^{15}N, ^{1}H]-NMR spectra of 250 µM [U-^{2}H, ^{15}N]-Skp in the absence (grey) and presence (red) of 750 µM α-synuclein. **b**, Residue-resolved NMR signal intensity ratios ($I_{rel} = I/I_0$) of Skp (250 µM) in the presence of three equivalents of α-synuclein measured at 310 K. The thin dashed lines indicate a significance level of one s.d. from the mean. The solid line represents an intensity ratio of 1. **c**, α-Synuclein induced intensity changes plotted on the Skp crystal structure (RCSB Protein Data Bank code (PDB) 1SG2)[32] and previously reported effects upon binding of its native client OmpX[10]. A decrease in the signal intensity of more than one s.d. is highlighted in blue, whereas an increase in signal intensity is highlighted in red. **d**, Overlay of two-dimensional [^{15}N, ^{1}H]-NMR spectra of 250 µM [U-^{2}H, ^{15}N]-Skp in the absence (grey) and presence (blue) of 500 µM BSA. **e**, Residue-resolved NMR signal intensity ratios ($I_{rel} = I/I_0$) of Skp (250 µM) in the presence of two equivalents of BSA measured at 310 K. The solid line represents an intensity ratio of 1. **f**, Overlay of two-dimensional [^{15}N, ^{1}H]-NMR spectra of 250 µM [U-^{2}H, ^{15}N]-TF(ΔRBD), a monomeric Trigger Factor (TF) variant that lacks its ribosome-binding and main dimerization domain (RBD), in the absence (grey) and presence (orange) of 750 µM α-synuclein. **g**, Residue-resolved NMR signal intensity ratios ($I_{rel} = I/I_0$) of 250 µM TF(ΔRBD) in the presence of three equivalents of α-synuclein measured at 298 K. The thin broken lines indicate a significance level of one s.d. from the mean. The thick line represents an intensity quotient of 1. **h**, Residue-resolved combined chemical-shift differences of the amide moieties. The broken line indicates a significance level of two s.d. from the mean. **i**, Significant chemical-shift changes (green) and intensity decrease (blue) plotted on the Trigger Factor structure (PDB 1W26)[33]. Comparison with the published Trigger Factor interaction sites of PhoA (orange)[34]. **j**, Overlay of two-dimensional [^{15}N, ^{1}H]-NMR spectra of 250 µM [U-^{2}H, ^{15}N]-TF(ΔRBD) in the absence (grey) and presence (blue) of 500 µM BSA. **k**, Residue-resolved NMR signal intensity ratios ($I_{rel} = I/I_0$) of TF(ΔRBD) (250 µM) in the presence of two equivalents of BSA measured at 298 K. The solid line represents an intensity ratio of 1. Experiments with α-synuclein (**a**, **f**) were done as duplicates yielding similar results, whereas control experiments with BSA (**d**, **j**) were performed once.
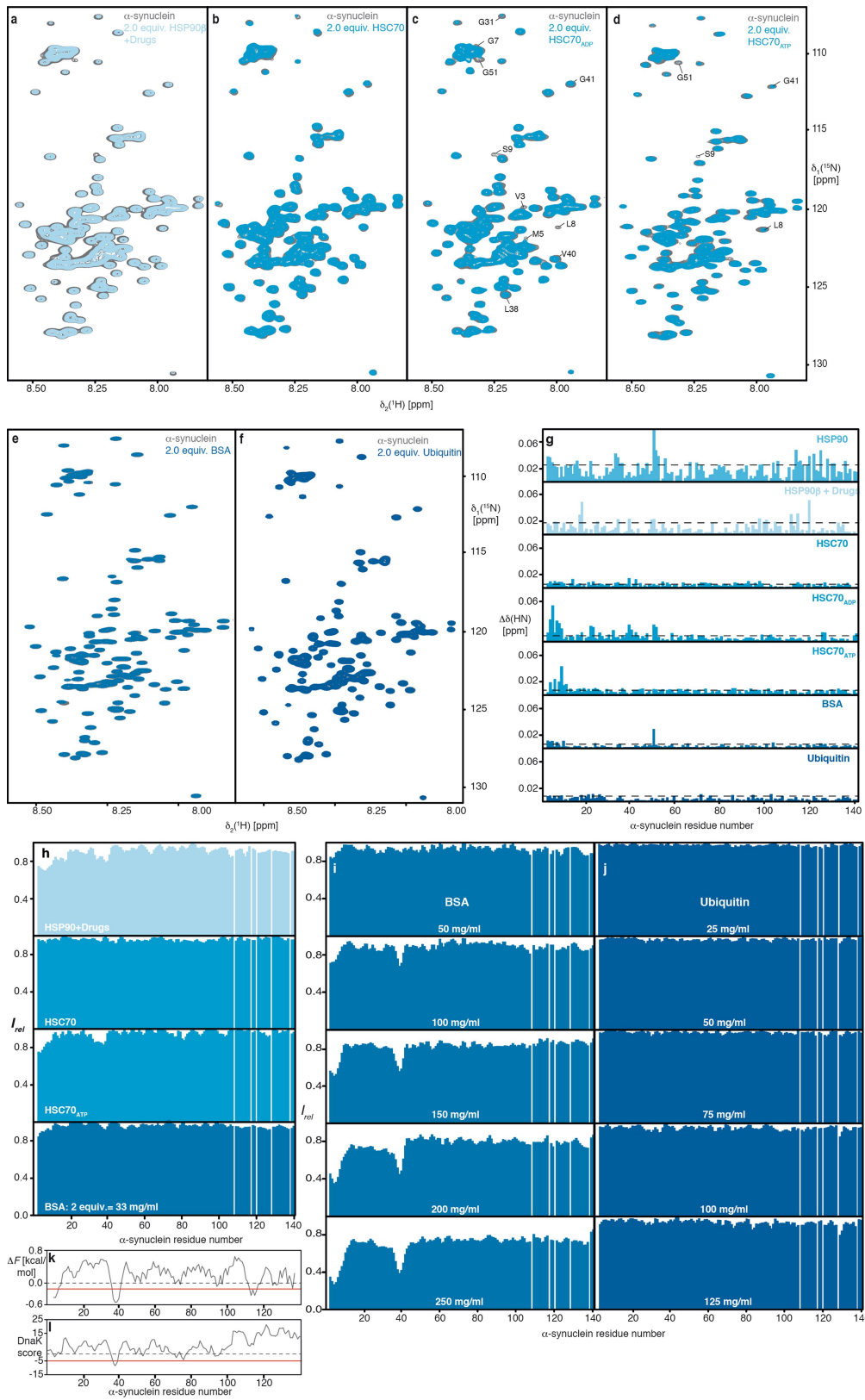
**Extended Data Fig. 3** | See next page for caption.

Extended Data Fig. 3 | Interaction between α-synuclein and mammalian proteins. a, Overlay of two-dimensional [^{15}N, ^{1}H]-NMR spectra of 25 μM [U-^{15}N]-α-synuclein in the absence (grey) and presence (light blue) of 50 μM inhibited HSP90β dimer. Measured in NMR buffer plus 5 mM MgCl$_2$, 5 mM ATP, 1 μM radicicol and 1 μM geldanamycin. **b**, Overlay of two-dimensional [^{15}N, ^{1}H]-NMR spectra of 100 μM [U-^{15}N]-α-synuclein in the absence (grey) and presence (light blue) of 200 μM HSC70. **c**, Overlay of two-dimensional [^{15}N, ^{1}H]-NMR spectra of 100 μM [U-^{15}N]-α-synuclein in the absence (grey) and presence (light blue) of 200 μM HSC70$_{ADP}$. Measured in NMR buffer plus 5 mM MgCl$_2$ and 5 mM ADP. **d**, Overlay of two-dimensional [^{15}N, ^{1}H]-NMR spectra of 100 μM [U-^{15}N]-α-synuclein in the absence (grey) and presence (light blue) of 200 μM HSC70$_{ATP}$. Measured in NMR buffer plus 5 mM MgCl$_2$ and 5 mM ATP. **e**, Overlay of two-dimensional [^{15}N, ^{1}H]-NMR spectra of 250 μM [U-^{15}N]-α-synuclein in the absence (grey) and presence (blue) of 500 μM (33 mg ml^{-1}) BSA. **f**, Overlay of two-dimensional [^{15}N, ^{1}H]-NMR spectra of 250 μM [U-^{15}N]-α-synuclein in the absence (grey) and presence (dark blue) of 500 μM of ubiquitin. **g**, Residue-resolved combined chemical-shift perturbations of amide moieties upon addition of HSP90β (cyan), inhibited HSP90β (light cyan), HSC70 (light blue), HSC70$_{ADP}$ (light blue), HSC70$_{ATP}$ (light blue), BSA (blue) and ubiquitin (dark blue). Broken lines indicate a significance level of two s.d. from the mean. **h**, Residue-resolved backbone amide NMR signal attenuation ($I_{rel} = I/I_0$) of α-synuclein caused by the addition of two equivalents of inhibited HSP90β (light cyan), HSC70 (light blue), HSC70$_{ATP}$ (light blue) and BSA (blue). **i**, Residue-resolved NMR signal attenuation ($I_{rel} = I/I_0$) of 100 μM [U-^{15}N]-α-synuclein upon addition of increasing BSA concentrations (50–250 mg ml^{-1}). **j**, Residue-resolved NMR signal attenuation ($I_{rel} = I/I_0$) of 50 μM [U-^{15}N]-α-synuclein upon addition of increasing ubiquitin concentrations (25–125 mg ml^{-1}). **k**, Local hydrophobicity of α-synuclein plotted against the amino acid sequence. ΔF are the free energies of transfer of the individual amino acids from an aqueous solution to its surface[35]. Hydrophobicity corresponds to negative ΔF values. An exponentially weighted seven-window average was applied to the raw data, with the edges contributing 50%. The red line indicates the average value of 1.5 s.d. from the mean, the chosen threshold for the identification of the most hydrophilic segments. **l**, Sequence-dependent DnaK score for α-synuclein derived from a computational DnaK prediction algorithm[36]. Regions of the primary sequence with scores less than −5 (red line) are predicted to bind DnaK, a bacterial homologue of HSC70. Experiments in **a**–**f** were done in duplicates with similar results.
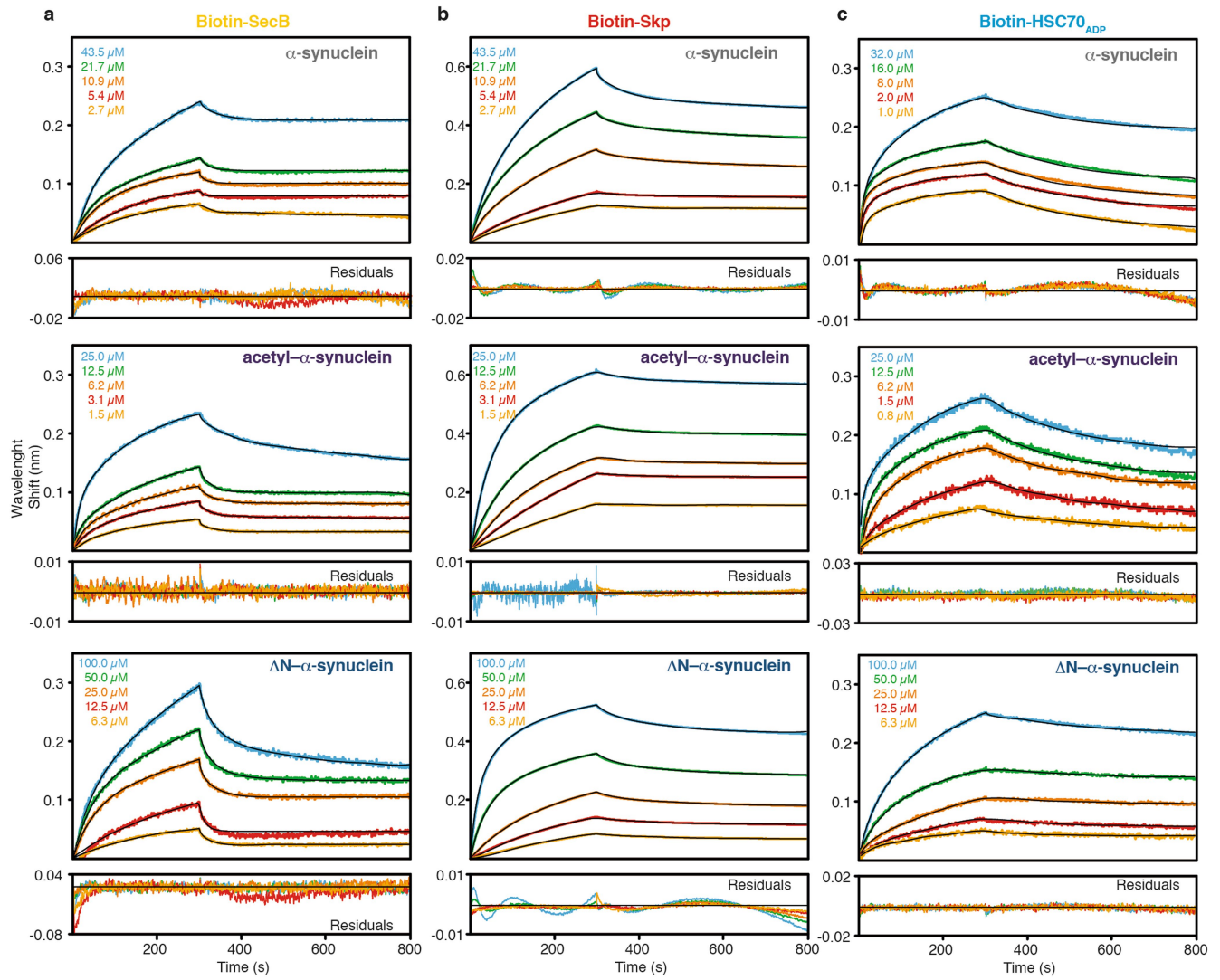
Extended Data Fig. 4 | Kinetic analysis of the interaction of the chaperones with α-synuclein variants. a–c, Kinetic analysis by bio-layer interferometry of biotinylated Skp (**a**), SecB (**b**) and HSC70$_{ADP}$ (**c**) to different α-synuclein variants (α-synuclein (top), acetyl-α-synuclein (middle) and ΔN-α-synuclein (bottom)). Black lines represent least-square fits to the data. The residuals of the fits are shown below each set of bio-layer interferometry curves. Each individual kinetic experiment was run twice in triplicates with similar results.
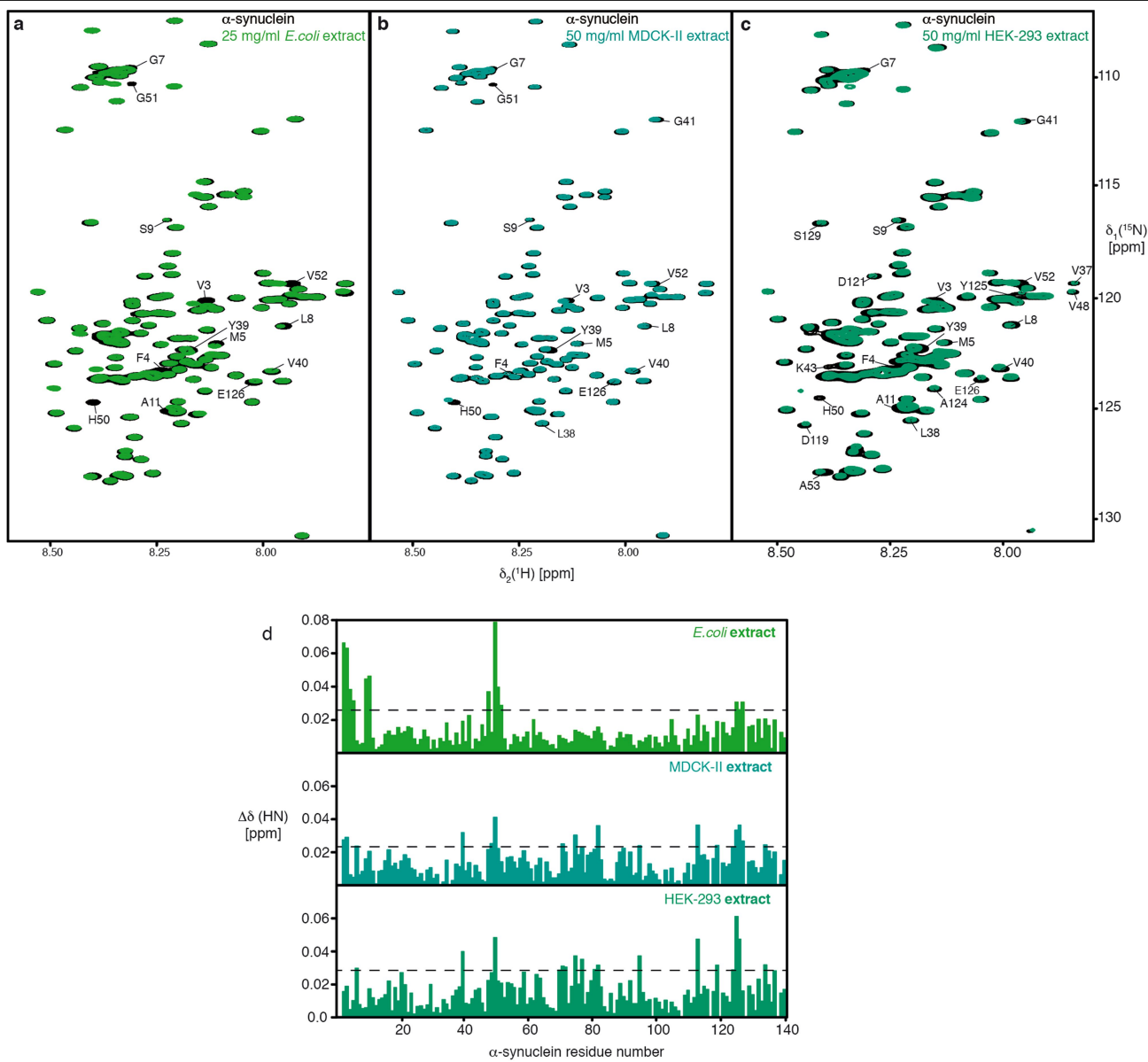
Extended Data Fig. 5 | Interaction between α-synuclein and cellular extracts. a, Overlay of two-dimensional [^{15}N, ^{1}H]-NMR spectra of 50 µM [U-^{15}N]-α-synuclein in the absence (black) and presence (green) of 25 mg ml^{-1} of $E. coli$ cell extract. **b**, Overlay of two-dimensional [^{15}N, ^{1}H]-NMR spectra of 50 µM [U-^{15}N]-α-synuclein in the absence (black) and presence of 50 mg ml^{-1} mammalian MDCK-II cell extract (blue-green). **c**, Overlay of two-dimensional [^{15}N, ^{1}H]-NMR spectra of 50 µM [U-^{15}N]-α-synuclein in the absence (black) and presence (green) of 50 mg ml^{-1} mammalian HEK293 cell extract. **d**, Residue-resolved combined chemical-shift perturbations of the α-synuclein amide moieties in $E. coli$ cell extract (green), mammalian MDCK-II cell extract (blue) and mammalian HEK293 cell extract (green), all relative to aqueous buffer. Broken lines indicate a significance level of two s.d. from the mean. Experiments in **a**–**c** were done in duplicates with similar results.

a

5 mg/ml LUVs

5 mg/ml LUVs + SecB

b

15 mg/ml LUVs

15 mg/ml LUVs + 2 equiv. SecB

15 mg/ml LUVs + 6 equiv. SecB

c

SecB

SecB + 2.5 mg/ml LUVs

SecB + 4.0 mg/ml LUVs

SecB + 6.25 mg/ml LUVs

SecB + 8.5 mg/ml LUVs

α-synuclein residue number

α-synuclein residue number

d

α-synuclein

Large unilamellar vesicle

Chaperone

e

Mean Volume [%]

Size distribution [nm]
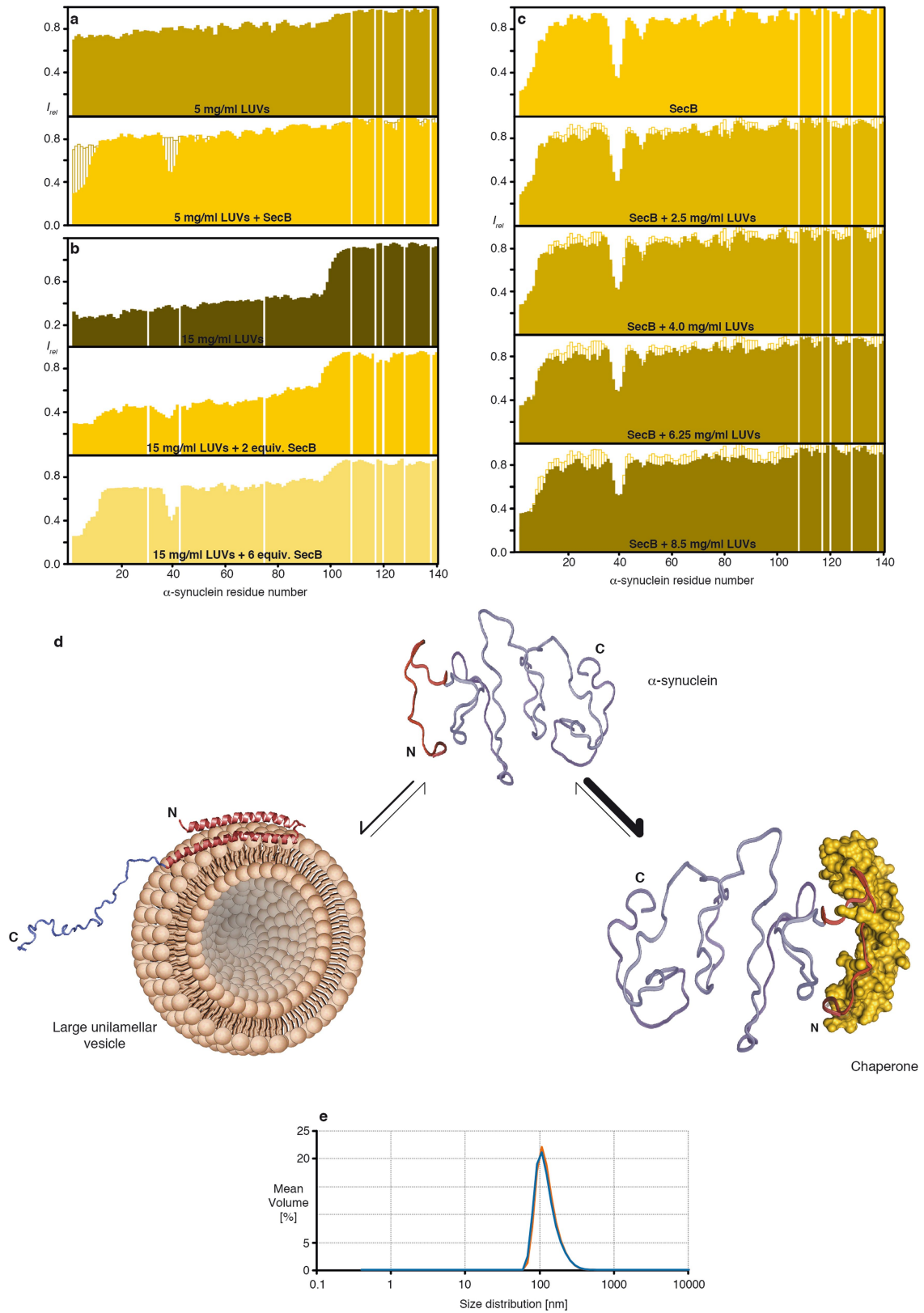
Extended Data Fig. 6 | See next page for caption.

Extended Data Fig. 6 | LUVs and the chaperone SecB compete for α-synuclein binding. a, Residue-resolved backbone amide NMR signal attenuation ($I_{rel} = I/I_0$) of α-synuclein caused by the addition of 5 mg ml^{-1} LUVs (125:1 molar ratio of lipid:protein; dark yellow) and after further addition of 2 equivalents of SecB (yellow). **b**, Residue-resolved backbone amide NMR signal attenuation ($I_{rel} = I/I_0$) of α-synuclein caused by the addition of 15 mg ml^{-1} LUVs (375:1 molar ratio lipid:protein; dark yellow) and after further addition of 2 and 6 equivalents of SecB, respectively (yellow), measured at 298 K. **c**, Residue-resolved backbone amide NMR signal attenuation ($I_{rel} = I/I_0$) of α-synuclein caused by the addition of 2 equivalents of SecB (yellow) and increasing amounts of LUVs with the following ratios: 2.5 mg ml^{-1}, 62.5:1; 4.0 mg ml^{-1}, 100:1; 6.25 mg ml^{-1}, 156:1; 8.5 mg ml^{-1}, 212.5:1. **d**, Schematic showing the conformational equilibrium of free α-synuclein, its chaperone-bound state and one possible conformation of its LUV-bound state (PDB 1XQ8)[19]. Notably, these observations are also in full agreement with related studies for HSP90[12] and HSP27[37]. **e**, Dynamic light scattering (DLS) measurements of LUVs prepared from pig brain polar lipids. Two independent preparations are shown in blue and orange, respectively, with an average diameter of 110 nm.
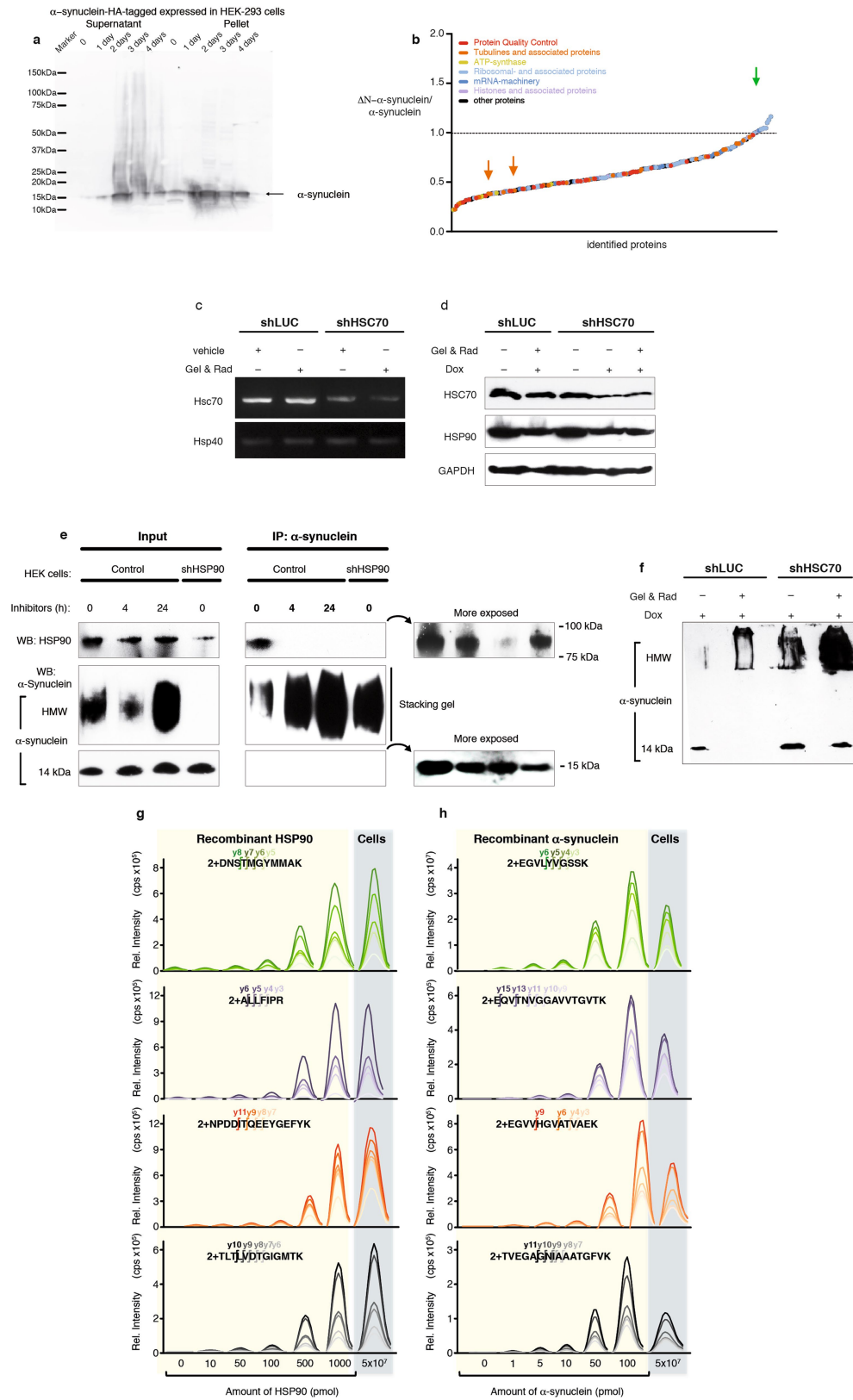
Extended Data Fig. 7 | See next page for caption.

**Extended Data Fig. 7 | Interaction of α-synuclein and chaperones in cells.**
a, Western blot analysis of the expression of α-synuclein fused to a C-terminal haemagglutinin (HA)-tag in HEK293 cells. The molecular mass marker and the band corresponding to α-synuclein–HA are indicated. With these samples, immunoprecipitation and subsequent mass-spectrometry analysis was performed (**b** and Fig. 2a). **b**, Intensity ratios of carboxy-terminally HA-tagged ΔN-α-synuclein and α-synuclein immunoprecipitation determined by relative quantitative mass-spectrometry analysis. Experiments were performed as duplicates in HEK293 cells. Identification of at least five peptides per protein was required for quantification. Data are mean. The dotted line represents an intensity ratio of 1. Proteins that belong to specific groups are highlighted in colours. The values for α-synuclein (green) as well as tubulin β4 and tubulin α1B (orange arrows from left to right) are indicated by coloured arrows.
c, Efficiency of HSC70 knockdown in HEK293 cells (constitutively expressing the T-Rex repressor) stably transfected with an inducible shRNA targeting *HSC70* mRNA (shHSC70). The image shows a representative semiquantitative reverse-transcription (RT)–PCR of *HSC70* mRNA in cells treated with doxycycline to induce shHSC70 and geldanamycin (Gel) and radicicol (Rad) for 24 h (+). Cells transfected with a control shRNA targeting firefly luciferase (shLUC) as well as semiquantification of an unrelated chaperone (HSP40) were included as negative and loading controls. **d**, Semiquantification of HSC70 and HSP90 protein levels by western blot. HEK293 cells (constitutively expressing the T-Rex repressor) stably transfected with shHSC70 and shLUC were grown in normal (−) or doxycycline-containing (+) medium for HSC70 knockdown. The cells were subsequently treated with vehicle (−) or geldanamycin and radicicol for HSP90 inhibition. The constitutively expressed protein GAPDH was assayed as loading control. **e**, Efficiency of the combined treatment of geldanamycin and radicicol in disrupting the α-synuclein–HSP90 interaction. HEK293 cells

were treated with geldanamycin and radicicol for 4 or 24 h and then electroporated with recombinant α-synuclein using the protocol for in-cell NMR experiments. Whole-cell lysates were collected and used in immunoprecipitation assays with anti-α-synuclein antibodies. The obtained precipitates were then resolved by SDS–PAGE and analysed by western blot using the indicated antibodies. In addition to HEK293 cells with normal levels of HSP90 (control cells), cells with reduced levels of HSP90 (shHSP90) were used to validate the HSP90 band. **f**, Inhibition of both HSP90 and HSC70 promotes aggregation of α-synuclein. The image shows a representative semiquantitative western blot of HSC70-depleted HEK293 cells treated with geldanamycin and radicicol. After 24 h of treatment, the cells were subjected to electroporation with recombinant α-synuclein and 4 h after electroporation the cells were collected and analysed by western blot. HMW and 14 kDa refer to high-molecular weight and monomeric α-synuclein species, respectively.
g, **h**, Quantification of intracellular levels of HSP90 and electroporated α-synuclein in HEK293 cells by parallel reaction monitoring mass spectrometry. A standard curve (contained in the yellow boxes) using increasing amounts of recombinant HSP90 (**g**) or α-synuclein (**h**) enables the relative quantification of the intracellular protein levels. As surrogates for intracellular protein levels, at least four tryptic peptides of HSP90 (**g**) or human α-synuclein (**h**) were quantified. Targeted peptides are shown at the top of each plot, and at least four transitions of the *y*-series of the product ions were monitored over the chromatographic separation of the peptides (different colours). The determined cellular concentrations of HSP90 and α-synuclein were 30 μM and 2.5 μM, respectively (see Supplementary Methods for details of this calculation). cps, counts per second. The original and uncropped gels of **a**, **c**–**f** can be found in Supplementary Fig. 1. Western blot and PCR experiments (**a**, **c**–**f**) were done in duplicates, with in similar results.
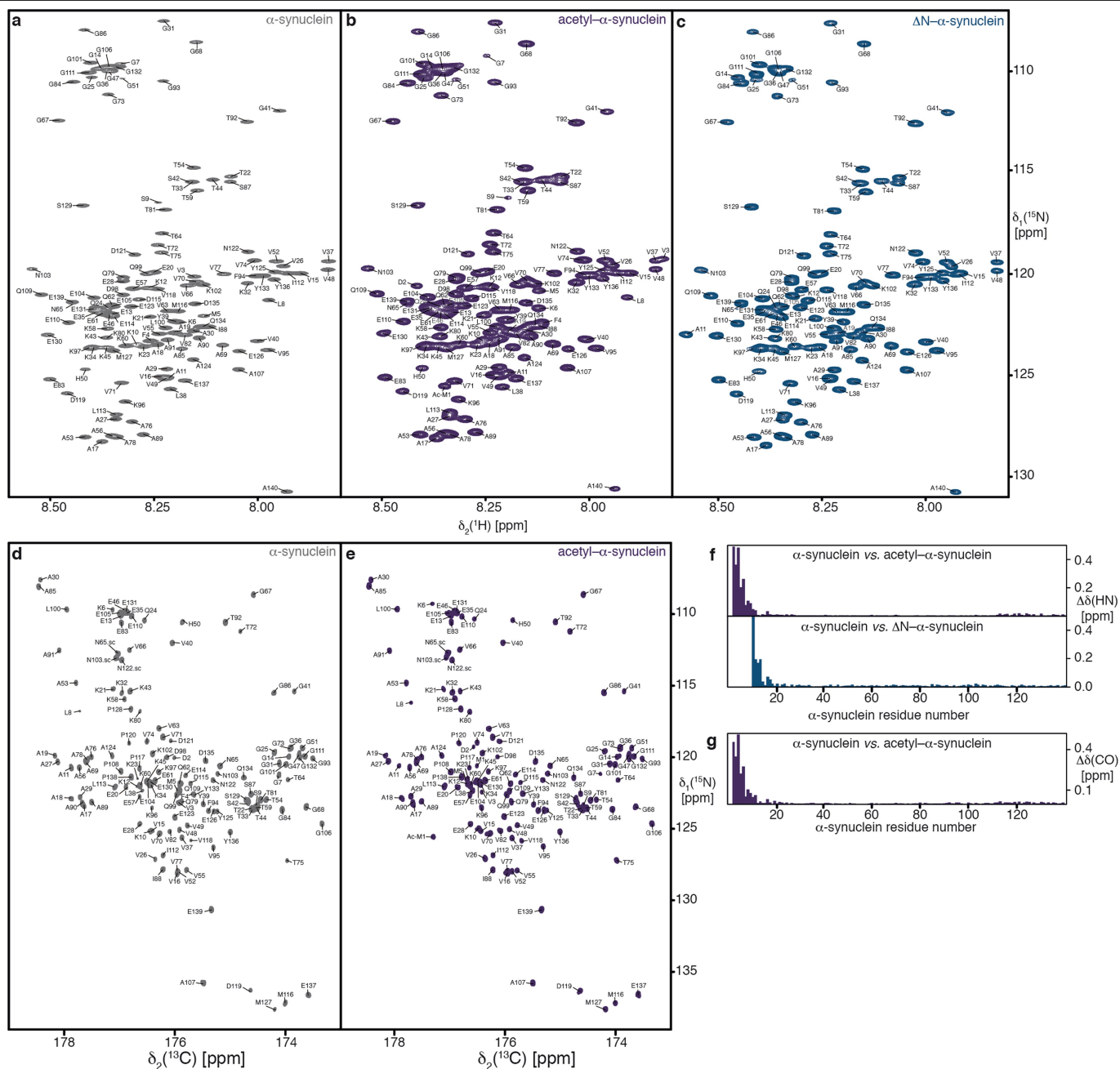
Extended Data Fig. 8 | Sequence-specific NMR-resonance assignments of α-synuclein variants. a–**c**, Two-dimensional [^{15}N, ^{1}H]-NMR spectra of 500 μM [U-^{13}C, ^{15}N]-α-synuclein (grey), 450 μM [U-^{13}C, ^{15}N]-acetyl-α-synuclein (dark violet) and 100 μM [U-^{15}N]-ΔN-α-synuclein (dark blue). The sequence-specific resonance assignments for wild-type as well as acetylated α-synuclein obtained from three-dimensional triple resonance experiments and from chemical-shift mapping of ΔN-α-synuclein are indicated. **d**, **e**, Two-dimensional [^{13}C, ^{15}N]-NMR spectra of 500 μM [U-^{13}C, ^{15}N]-α-synuclein (grey) and 450 μM [U-^{13}C, ^{15}N]-acetyl-α-synuclein (dark violet). The sequence-specific resonance assignments for

wild-type and acetylated α-synuclein obtained from three-dimensional triple resonance experiments are indicated. **f**, Residue-resolved combined chemical-shift perturbations of the amide moieties for acetyl-α-synuclein (dark violet) and ΔN-α-synuclein (dark blue) versus wild-type α-synuclein. **g**, Residue-resolved combined chemical-shift difference of the carbonyl-amide moieties for acetyl-α-synuclein (dark violet) versus wild-type α-synuclein. [^{15}N, ^{1}H]-NMR spectra in **a**–**c** were measured five times and [^{13}C, ^{15}N]-NMR spectra (**d**, **e**) were measured in duplicates, all yielding similar results.
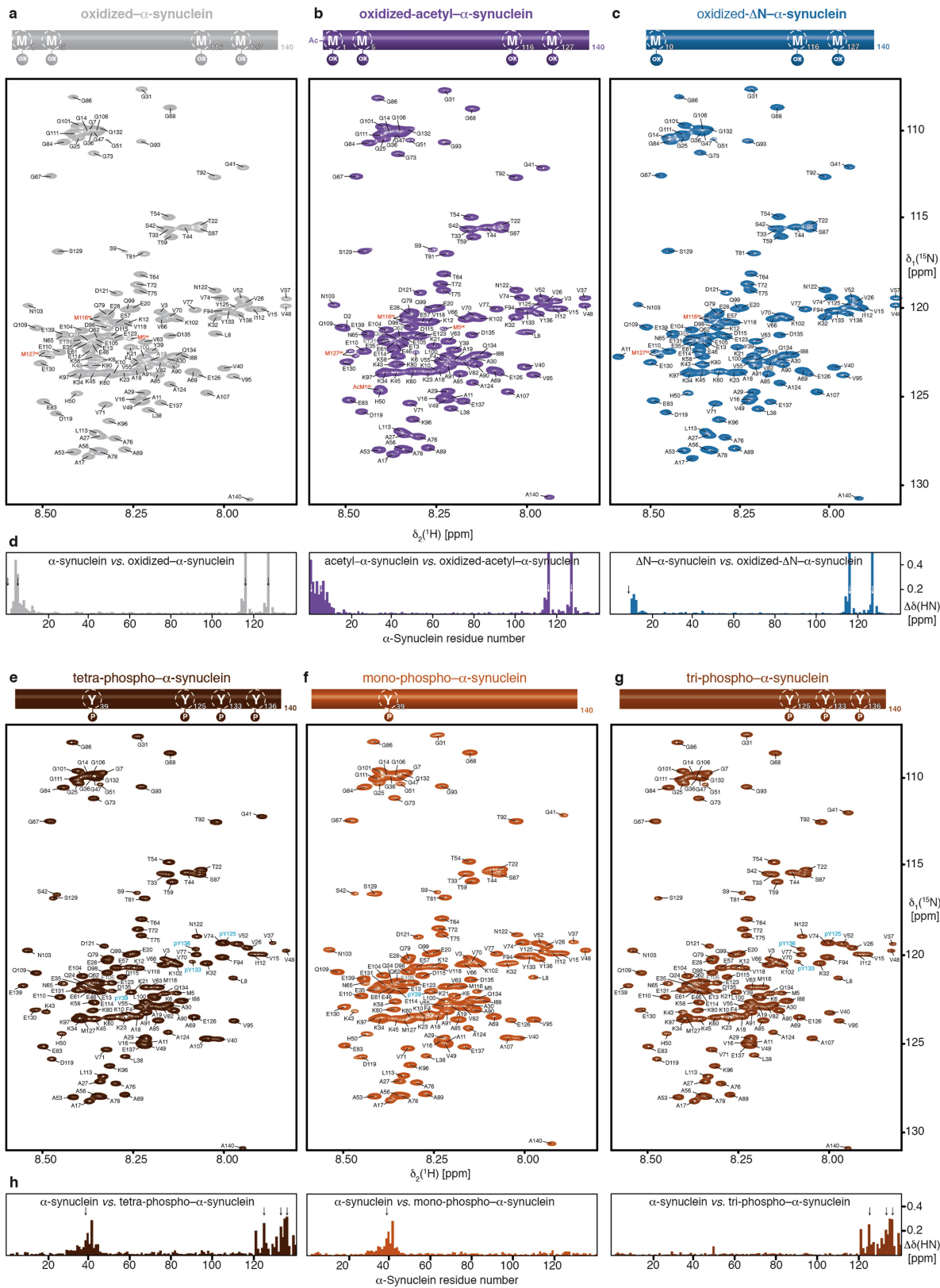
Extended Data Fig. 9 | See next page for caption.

Article

Extended Data Fig. 9 | Sequence-specific NMR-resonance assignments of methionine-oxidized and tyrosine-phosphorylated α-synuclein variants. **a**–**c**, Two-dimensional [^{15}N, ^{1}H]-NMR spectra of 100 μM oxidized [U-^{15}N]-α-synuclein (light grey), 100 μM oxidized [U-^{15}N]-acetyl-α-synuclein (violet) and 100 μM oxidized [U-^{15}N]-ΔN-α-synuclein (blue). The sequence-specific resonance assignments from chemical-shift mapping and published assignments of the oxidized state[23] are indicated. Oxidized methionines are highlighted in red. **d**, Residue-resolved combined chemical-shift differences of the amide moieties for oxidized α-synuclein (light grey), oxidized acetyl-α-synuclein (violet) and oxidized-ΔN-α-synuclein (blue) relative to their respective reduced states. Colours as in **a**–**c**. Arrows indicate the positions of the oxidized methionines. **e**–**g**, Two-dimensional [^{15}N, ^{1}H]-NMR spectra of 50 μM [U-^{15}N]-mono-phospho-α-synuclein (red-brown), 50 μM [U-^{15}N]-tri-phospho-α-synuclein (brown) and 50 μM [U-^{15}N]-tetra-phospho-α-synuclein (dark brown). The sequence-specific resonance assignments based on published assignments for phosphorylated α-synuclein are indicated[24]. Phosphorylated residues are highlighted in cyan. **h**, Residue-resolved combined chemical-shift differences of the amide moieties for the phosphorylated α-synuclein variants relative to wild-type α-synuclein. Colours as in **e**–**g**. Arrows indicate the positions of the phosphorylated tyrosines. [^{15}N, ^{1}H]-NMR spectra of the different modified α-synuclein variants were measured several times (n = 4) yielding similar results.
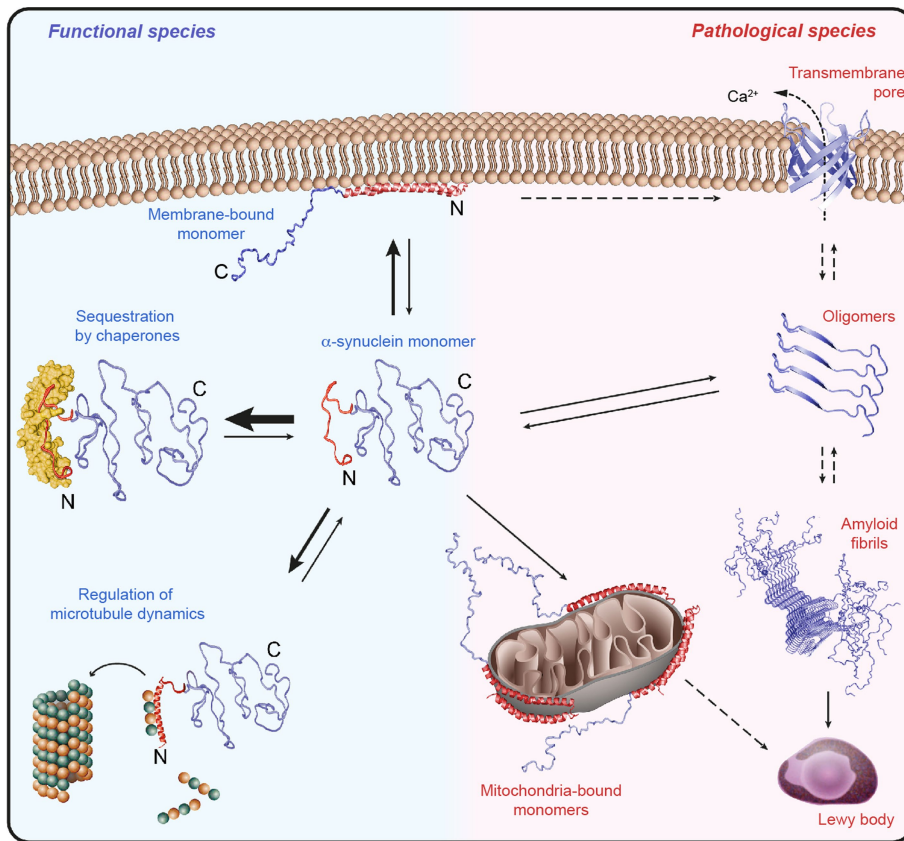
Extended Data Fig. 10 | Mechanism of chaperone-controlled regulation of α-synuclein function, conformation and localization in mammalian cells. Cellular chaperones (yellow) interact with the N-terminal segment of α-synuclein (red), thus actively regulating its functional species by shifting conformational equilibria. Impairment of the natural α-synuclein–chaperone ratio or abrogation of the α-synuclein–chaperone interaction by post-translational modifications can lead to the formation of pathological species, including the accumulation of α-synuclein at mitochondria.

Corresponding author(s): Sebastian Hiller, Björn M. Burmann, Roland Riek

Last updated by author(s): Sep 22, 2019

Reporting Summary

Nature Research wishes to improve the reproducibility of the work that we publish. This form provides structure for consistency and transparency in reporting. For further information on Nature Research policies, see Authors & Referees and the Editorial Policy Checklist.

Statistics

For all statistical analyses, confirm that the following items are present in the figure legend, table legend, main text, or Methods section.

n/a	Confirmed	
☐	☒	The exact sample size (*n*) for each experimental group/condition, given as a discrete number and unit of measurement
☐	☒	A statement on whether measurements were taken from distinct samples or whether the same sample was measured repeatedly
☒	☐	The statistical test(s) used AND whether they are one- or two-sided *Only common tests should be described solely by name; describe more complex techniques in the Methods section.*
☒	☐	A description of all covariates tested
☒	☐	A description of any assumptions or corrections, such as tests of normality and adjustment for multiple comparisons
☒	☐	A full description of the statistical parameters including central tendency (e.g. means) or other basic estimates (e.g. regression coefficient) AND variation (e.g. standard deviation) or associated estimates of uncertainty (e.g. confidence intervals)
☒	☐	For null hypothesis testing, the test statistic (e.g. F, t, r) with confidence intervals, effect sizes, degrees of freedom and P value noted *Give P values as exact values whenever suitable.*
☒	☐	For Bayesian analysis, information on the choice of priors and Markov chain Monte Carlo settings
☒	☐	For hierarchical and complex designs, identification of the appropriate level for tests and full reporting of outcomes
☒	☐	Estimates of effect sizes (e.g. Cohen's *d*, Pearson's *r*), indicating how they were calculated

Our web collection on statistics for biologists contains articles on many of the points above.

Software and code

Policy information about availability of computer code

Data collection	NMR data were collected on Bruker spectrometers operated with TOPSPIN 3.0-3.5.
Data analysis	NMR data were processed with PROSA and analyzed with CARA. MS data were analyzed with Skyline (MacCoss, Version 3.7).

For manuscripts utilizing custom algorithms or software that are central to the research but not yet described in published literature, software must be made available to editors/reviewers. We strongly encourage code deposition in a community repository (e.g. GitHub). See the Nature Research guidelines for submitting code & software for further information.

Data

Policy information about availability of data

All manuscripts must include a data availability statement. This statement should provide the following information, where applicable:
- Accession codes, unique identifiers, or web links for publicly available datasets
- A list of figures that have associated raw data
- A description of any restrictions on data availability

The data that support the findings of this study are available from the corresponding authors upon request.

Field-specific reporting

Please select the one below that is the best fit for your research. If you are not sure, read the appropriate sections before making your selection.

☒ Life sciences   ☐ Behavioural & social sciences   ☐ Ecological, evolutionary & environmental sciences

For a reference copy of the document with all sections, see nature.com/documents/nr-reporting-summary-flat.pdf

Life sciences study design

All studies must disclose on these points even when the disclosure is negative.

Sample size	No statistical methods were used to predetermine sample size. Sample sizes were chosen in agreement with established procedures in the field.
Data exclusions	No data was excluded from the analyses
Replication	Experiments were replicated to ensure reproducibility of the findings. The number of independent replicates for each experiment are specified in the respective Figure captions. All attempts at replication were successful.
Randomization	The experiments were not randomized, in agreement with established procedures in the field.
Blinding	The investigators were not blinded to allocation during experiments and outcome assessment, in agreement with established procedures in the field.

Reporting for specific materials, systems and methods

We require information from authors about some types of materials, experimental systems and methods used in many studies. Here, indicate whether each material, system or method listed is relevant to your study. If you are not sure if a list item applies to your research, read the appropriate section before selecting a response.

Materials & experimental systems

n/a	Involved in the study
☐	☒ Antibodies
☐	☒ Eukaryotic cell lines
☒	☐ Palaeontology
☒	☐ Animals and other organisms
☒	☐ Human research participants
☒	☐ Clinical data

Methods

n/a	Involved in the study
☒	☐ ChIP-seq
☒	☐ Flow cytometry
☒	☐ MRI-based neuroimaging

Antibodies

Antibodies used	Mouse anti-alpha-Synuclein Abcam Cat#: ab27766, RRID: AB_727020, 1:1000 for Western blot and Immunofluorescence Rabbit anti-alpha-Synuclein CellSignaling Cat#: 2642, RRID: AB_10695412, 1:1000 for Western blot and Immunofluorescence Mouse anti-Hsc70 Abcam Cat#: ab2788, RRID: AB_303301, 1:1000 for Western blot Mouse anti-Hsp90 Beta Abcam Cat#: ab53497, RRID: AB_881097, 1:3000 for Western blot Rabbit anti-COX IV ProteinTech Cat#: 11242-1-AP, RRID: AB_2085278, 1:500 for Immunofluorescence Rabbit anti-COX IV Abcam Cat#: ab16056, RRID: AB_443304, 1:1000 for Immunofluorescence Mouse anti-GAPDH Thermo Fischer Scientific Cat#: GA1R, RRID: AB_10751612, 1:5000 for Western blot
Validation	Mouse anti-alpha-Synuclein Abcam Cat#: ab27766, validated by Abcam Rabbit anti-alpha-Synuclein CellSignaling Cat#: 2642, validated by CellSignaling and by our lab Mouse anti-Hsc70 Abcam Cat#: ab2788, validated by Abcam Mouse anti-Hsp90 Beta Abcam Cat#: ab53497, validated by Abcam Rabbit anti-COX IV ProteinTech Cat#: 11242-1-AP, validated by Proteintech Rabbit anti-COX IV Abcam Cat#: ab16056, validated by Abcam Mouse anti-GAPDH Thermo Fischer Scientific Cat#: GA1R, validated by Thermo Fischer Scientific

Eukaryotic cell lines

Policy information about cell lines

Cell line source(s)	Flp-In™ 293 cells were purchased from Thermo Fisher Scientific (R75007), HEK-293 were purchased from the American Type Culture Collection (CRL-1573).
Authentication	The authenticity of the cells was provided by Thermo Fisher Scientific and the American Type Culture Collection upon purchase. We have not authenticated these cell lines.
Mycoplasma contamination	The cells were tested for mycoplasma contamination every four weeks. Only mycoplasma-free cultures were used for the experiments.
Commonly misidentified lines (See ICLAC register)	No commonly misidentified cells were used.